

Supplementary Information

Anisotropic sol-gel transition and morphological aspects of a hierarchical network of nematic gel and a superimposed photopolymer

G.V. Varshini,^a D. S. Shankar Rao,^{a*} and S. Krishna Prasad^a

^aCentre for Nano and Soft Matter Sciences, Shivanapura, Bangalore 562162, India

*raoshankards@gmail.com

Contents

- 1) Figure SI-1: Molecular structure and transition temperature of the materials used.
- 2) Figure SI-2: Schematic diagram for the haze measurement.
- 3) Figure SI-3: Log-log plot of number of boxes (N) vs. box size (d).
- 4) **Fractal dimension analysis**
- 5) Figure SI-4: Binarisation of the SEM image for the N-P case, performed with manual thresholding.
- 6) Figure SI-5: Binarisation of the SEM image for the G-P case, performed with manual thresholding.
- 7) Figure SI-6: Variation of fractal dimension with grid rotation.
- 8) Figure SI-7: Variation of T_{NI} with X_{RM} for G-P, N-P and I-P cases.
- 9) Figure SI-8: Thermal variation of $\epsilon_{||}$ and ϵ_{\perp} for (a) G-P, (b) N-P and (c) I-P samples for representative concentrations.
- 10) Figure SI-9: Raw profiles of voltage dependence of permittivity for $X_{RM} = 1.5$ (G-P case) at 50 °C and 30 °C.
- 11) Table SI-1: X_{RM} dependence of V_{th} for G-P, N-P and I-P samples at 50 °C and 30 °C.
- 12) Table SI 2: X_{RM} dependence of K_{11} for G-P, N-P and I-P samples at 50 °C and 30 °C.
- 13) Figure SI-8: Electro-optical switching studies of $X_{RM} = 2$ for G-P and I-P samples in nematic and gel phase.
- 14) Table SI -3: τ_{on} and τ_{off} values for G-P, N-P and I-P samples at temperatures 50 °C and 30 °C.

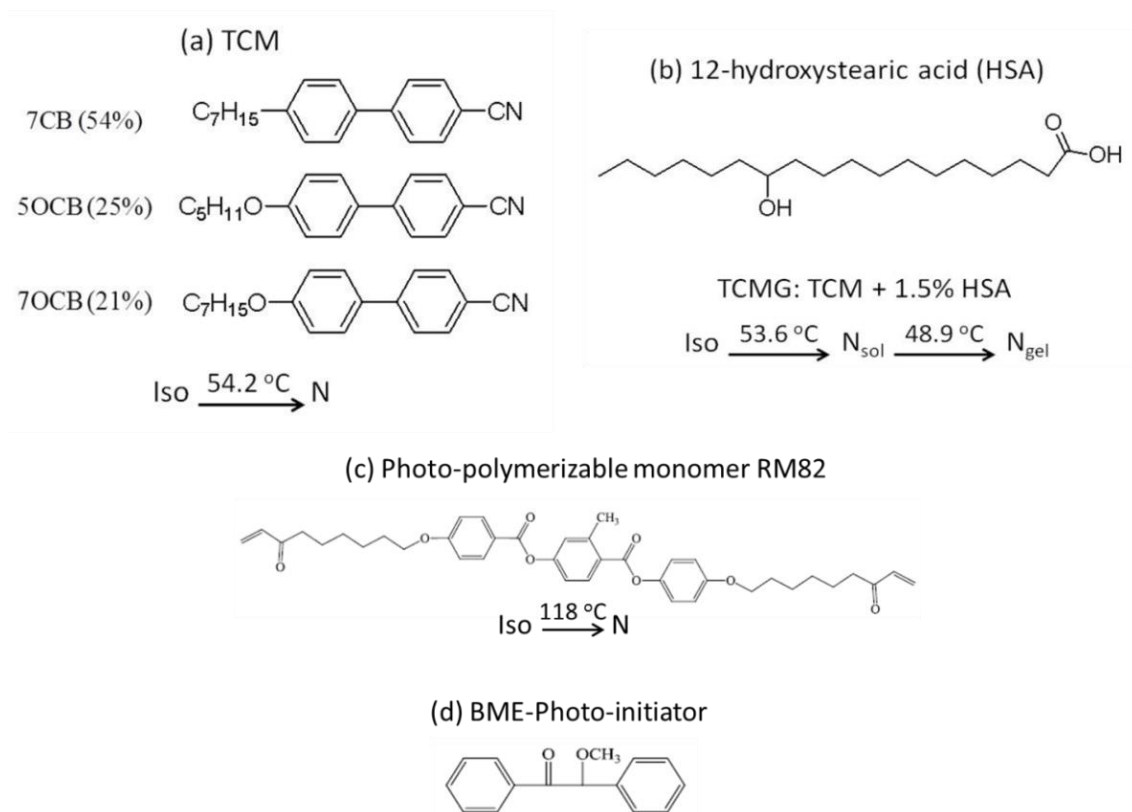


Figure SI-1: Molecular structure of the materials used: (a) Host TCM, a 3- component mixture exhibiting the nematic phase over a wide temperature range, and (b) Low molecular weight organic gelator, 12-hydroxystearic acid (HSA) and the composition of the mixture (TCMG) that exhibits the sol-gel transition. The transition temperatures for TCMG are for the “bulk” sample. (c) Photo-polymerisable monomer-RM82 and (d) Photo-initiator-BME, employed to initiate the polymerisation process.

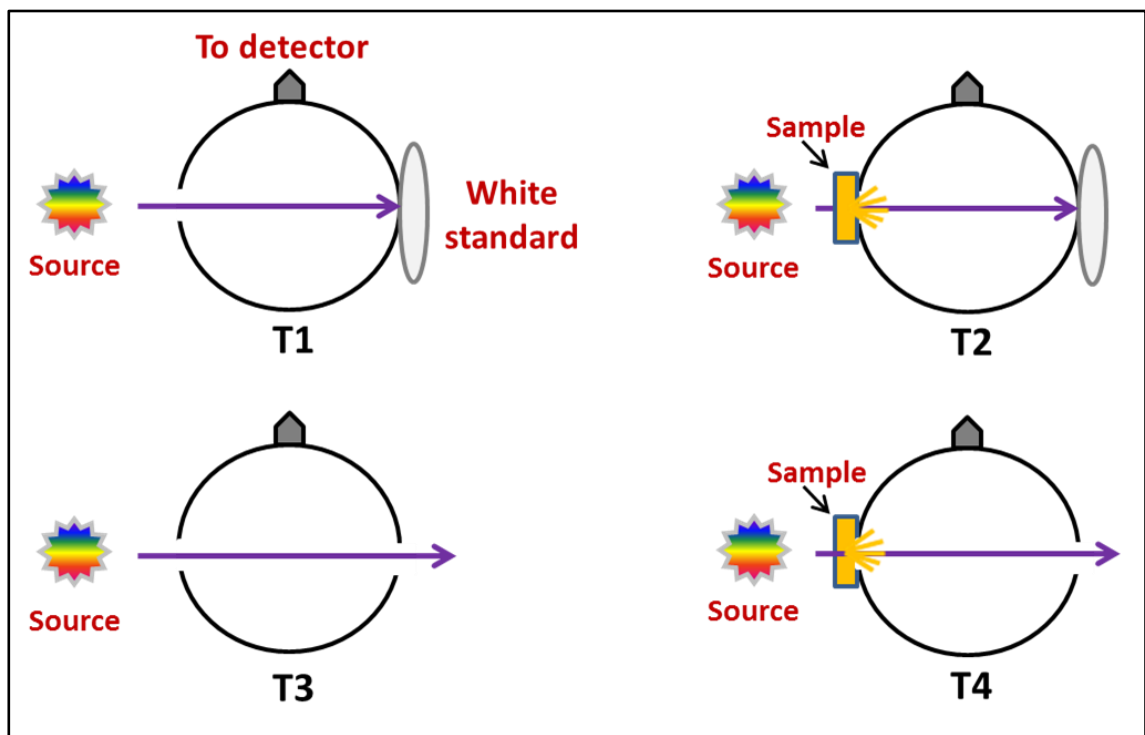


Figure SI-2: Schematic diagram representing the measurement of transmittance in four different configurations through which haze is calculated.

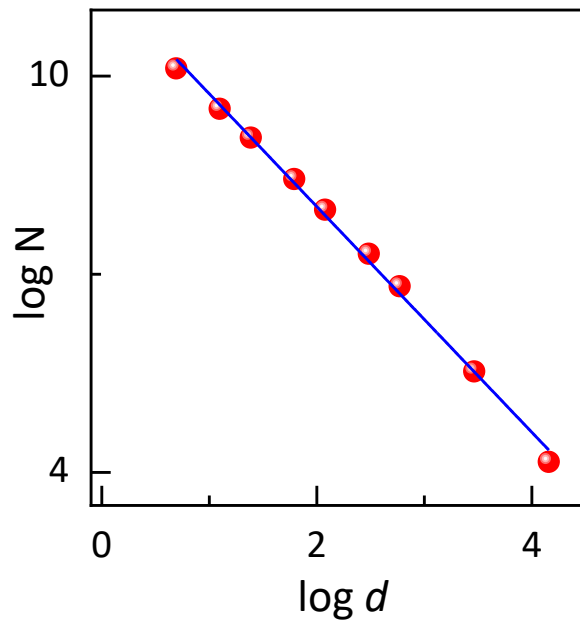


Figure SI-3: The variation of number of boxes (N) vs. box size (d) for the N-P sample with $X_{RM} = 3$, at a magnification of 15×10^3 . The slope of the line determines the fractal dimension D_f .

Fractal dimension analysis

Binary versions of the SEM images were generated using the ‘Make Binary’ option in the ‘ImageJ’ software. This conversion results in a black network on a white background with complete network being converted, not just the edges. At low magnifications although there could be an apparent feeling that only the edges of the network are seen, it is indeed not so. In fact, Fig 8 (d) clearly shows that whole network is being converted to black including the edges. The procedure employed was validated by three different means, the first of which was by performing the analyses with another well-known software, Fractalyse. Figures 9(a) and (b) the good agreement between the values obtained from the two software packages.

The second check was done by manually changing the threshold: Figures - 7(c) and 8(c) were considered for this comparison. The manually binarised images of these figures are shown in Figures SI-4(b) and 5(b). The manual-threshold method yielded a fractal dimension of 1.78 ± 0.09 and 1.77 ± 0.08 for the figures 7(c) and 8(c), respectively which agree, within the errors, with those obtained from the automatic-threshold method (1.72 ± 0.10 and 1.69 ± 0.09). The third check was done by performing the analysis on an image from the literature (I. Dierking, J. Phys. D: Appl. Phys., 35, 2520, ((2002), reporting fractal dimension features for a polymer-liquid crystal system. Our analysis for this image yielded a value of 1.84 ± 0.01 , in excellent agreement with a value of 1.85 reported in Ref. 43. It may be noted that the error bar for the analysis of this literature image, is much smaller than those for images from our experiments, perhaps indicating the complexity of the network in the present case. As a final check we also employed the modified box counting method, as detailed out in the main manuscript, the associated figure of which is given in Figure SI-6.

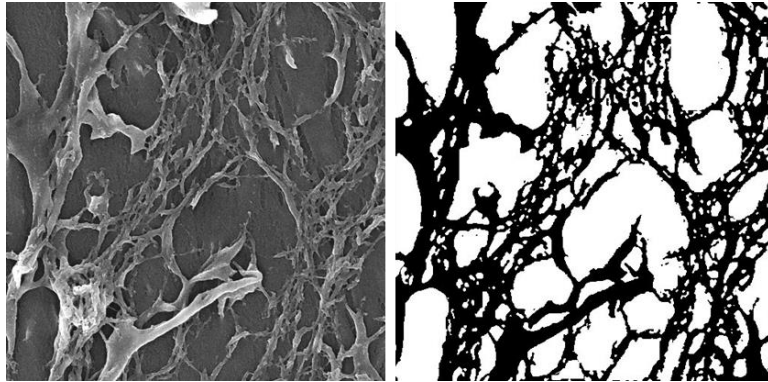


Figure SI-4: Binarisation of the SEM image for $X_{RM} = 3$ at a magnification of 15×10^3 for the N-P case, performed with manual thresholding.

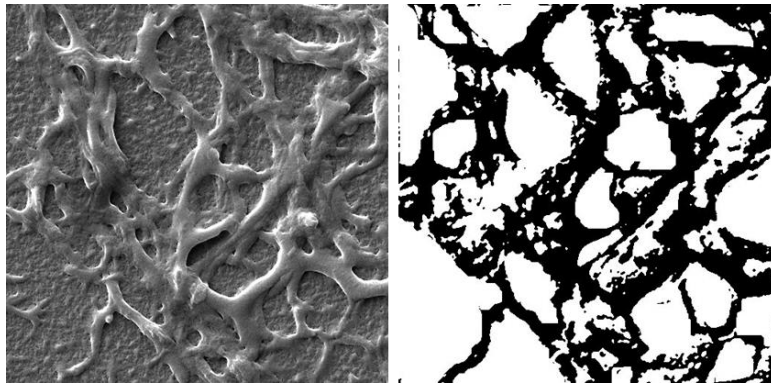


Figure SI-5: Binarisation of the SEM image for $X_{RM} = 3$ at a magnification of 15×10^3 for the G -P case, performed with manual thresholding.

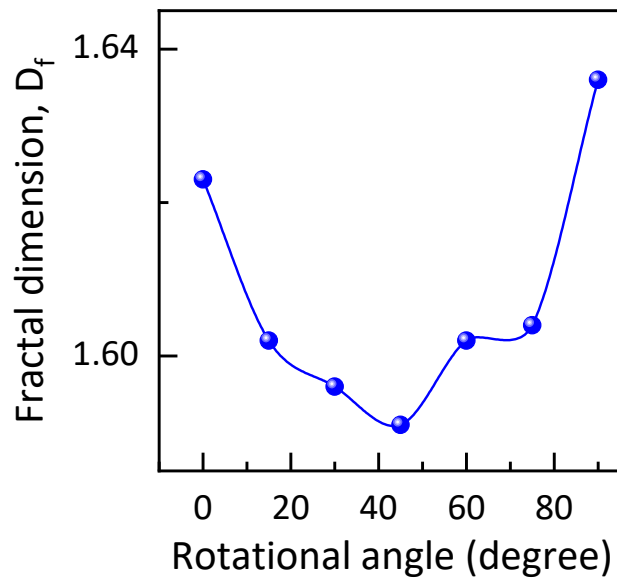


Figure SI-6: Variation of fractal dimension with grid rotation for G-P sample with a magnification of 15×10^3 .

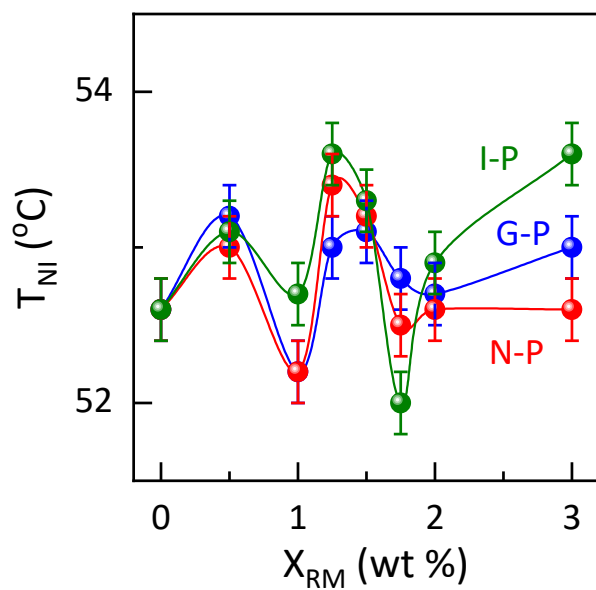


Figure SI-7: The variation of T_{NI} with different X_{RM} shown for G-P, N-P and I-P cases. The T_{NI} values are seen to be marginally affected (< 1 K).

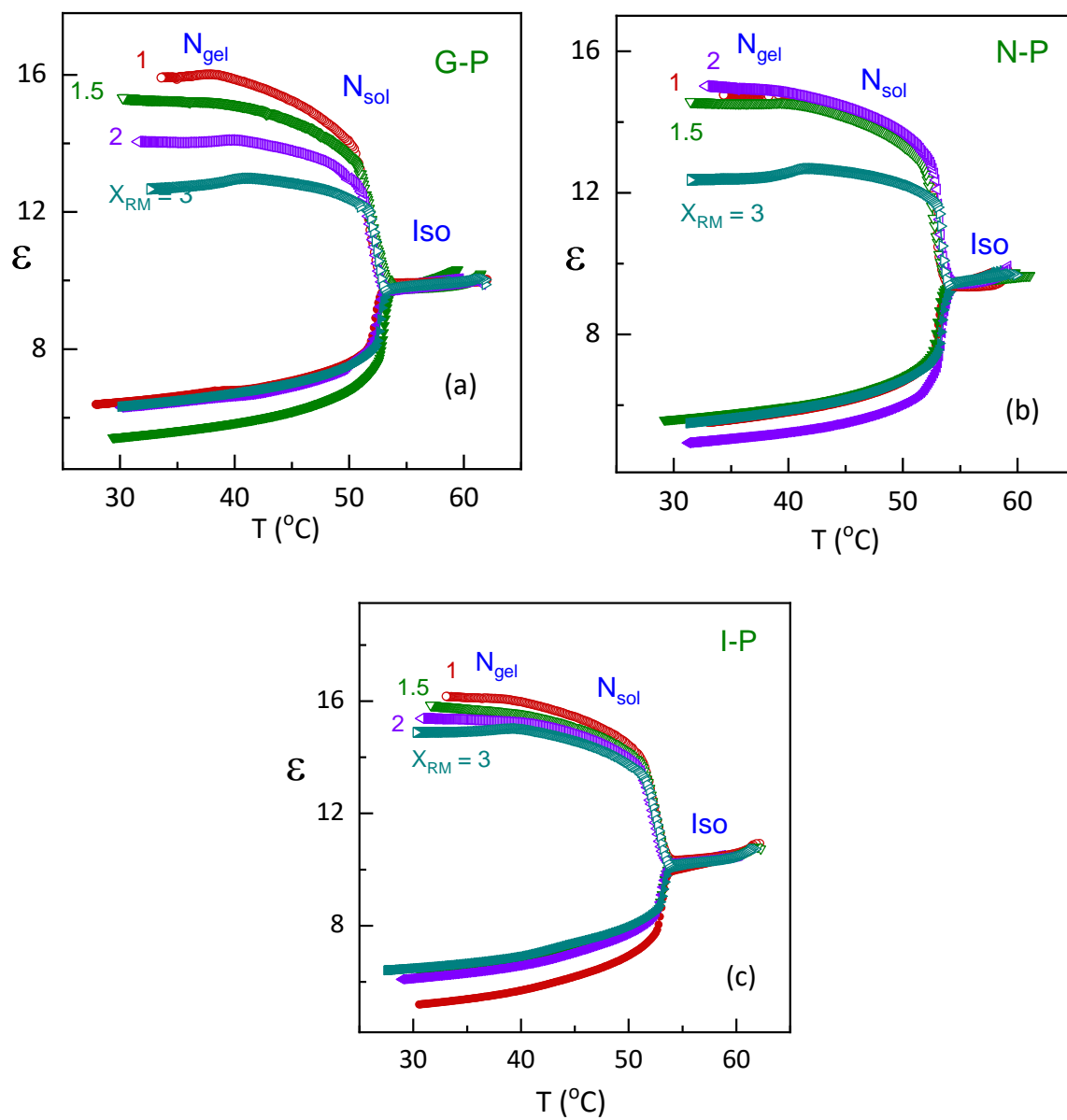


Figure SI-8: Thermal variation of ϵ_{\parallel} and ϵ_{\perp} for (a) G-P, (b) N-P and (c) I-P samples for representative concentrations. It is seen that for I-P, permittivity variations with varied X_{RM} are smaller compared to G-P and N-P.

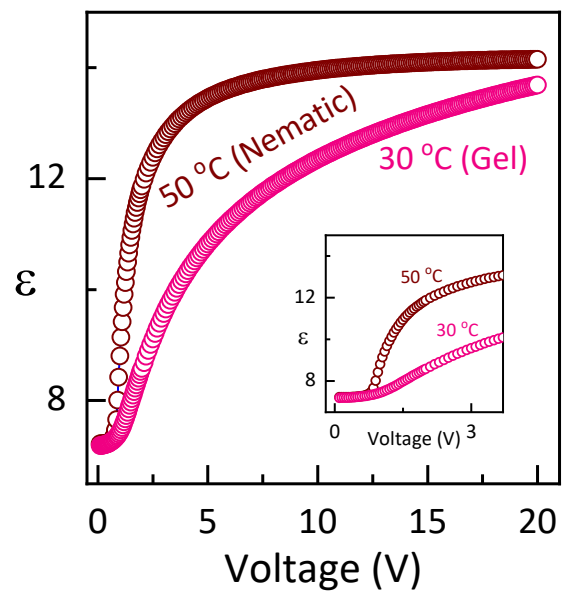


Figure SI-9: Raw profiles of voltage dependence of permittivity for $X_{RM} = 1.5$ (G-P case) at 50 °C and 30 °C. Inset represents the enlarged view of ϵ vs V showing increased threshold value in the gel phase.

Table SI-1: Concentration dependence of V_{th} (with an error of 0.1V) for G-P, N-P and I-P samples at 50 °C and 30 °C. The values are highly non-monotonic with varied X_{RM} but show a slightly higher threshold voltage at lower temperature.

X_{RM}	V_{th} (V) at 50 °C			V_{th} (V) at 30 °C		
	G-P	N-P	I-P	G-P	N-P	I-P
0*		0.68			0.92	
0.5	0.76	0.73	0.73	0.94	1.08	1.27
1	0.61	0.63	0.66	0.78	0.63	0.69
1.25	0.81	0.74	0.75	0.84	0.85	0.75
1.5	0.78	0.8	0.73	0.93	0.78	0.84
1.75	0.84	0.77	0.86	0.91	0.74	0.92
2	0.81	0.86	0.61	1.05	0.84	0.86
3	0.71	0.79	0.64	0.86	-	0.88

*Has no polymer content and the numbers represents the values obtained in N_{sol} and N_{gel} phase.

Table SI 2: Concentration dependence of K_{11} for G-P, N-P and I-P samples at 50 °C and 30 °C. The values are highly non-monotonic with varied X_{RM} but showcases higher splay constant at lower temperature.

X_{RM}	K_{11} (pN) at 50 °C			K_{11} (pN) at 30 °C		
	G-P	N-P	I-P	G-P	N-P	I-P
0*		2.9			6.9	
0.5	3.8	3.4	3.5	5.8	10.2	13.8
1	2.2	2.2	2.4	3.4	1.8	2.4
1.25	4.3	3.7	3.3	2	5.1	2.9
1.5	3.8	4	3	6	2.8	4.7
1.75	4.6	3.5	3.7	5.1	3.3	7
2	3.7	4.5	1.6	4.2	2.8	4.4
3	2.7	3.2	1	2.9	-	4.5

*Has no polymer content and the numbers represents the values obtained in N_{sol} and N_{gel} phase.

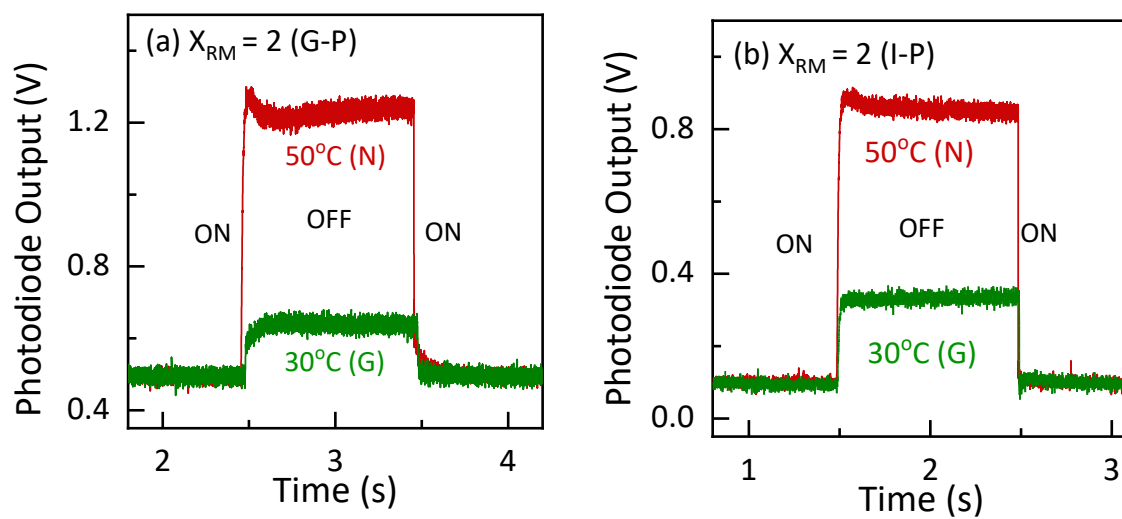


Figure SI-10: Electro-optical switching studies of $X_{RM} = 2$ for G-P and I-P samples in nematic and gel phase. At 30 °C (gel), as scattering is higher, the contrast between voltage on and off is less compared to 50 °C (nematic).

Table SI -3: Electro-optical response time (τ_{on} and τ_{off}) (in ms) values for G-P, N-P and I-P samples at temperatures 50 °C and 30 °C depicting N_{sol} and N_{gel} phase respectively.

X_{RM}	G-P				N-P				I-P			
	50 (°C)		35 (°C)		50 (°C)		35 (°C)		50 (°C)		35 (°C)	
	τ_{on}	τ_{off}										
0*					1.2	11.2	3.5	14.1				
0.5	1.1	6.4	1.8	10.9	2.2	5.5	6.1	49.4	1.1	8.2	23	3.1
1.5	2.1	4.7	3.4	6.6	15.1	5.3	8	5.7	1.3	10.9	1.5	20.6
2	8.2	16.2	8.8	25.1	1.3	19.5	-	-	0.8	16.5	1	15.6

*Has no polymer content and the numbers represents the values obtained in N_{sol} and N_{gel} phase.